Int. J. Heat Mass Transfer. Vol. 12, pp. 549–570. Pergamon Press 1969. Printed in Great Britain

THE EFFECT OF THERMAL CONDUCTIVITY OF THE PACKING MATERIAL ON TRANSIENT HEAT TRANSFER IN A FIXED BED

D. HANDLEY and P. J. HEGGS†
Department of Chemical Engineering, The University of Leeds, England

(*Received* 24 *February* 1968 *and in revised form* 26 *November* 1968)

Abstract— The mathematical equations describing transient heat transfer between the fluid flowing through a fixed bed of packing are formulated for the situations where (1) there is resistance to heat transfer within the solid phase and (2) there is thermal conduction in the solid phase along the direction of fluid flow.

Numerical analysis is presented for a computer solution of these equations and a parametric investigation of the models is used to show that the values of certain dimensionless groups arising from the mathematical formulation may be used to define the range of conditions under which the alternative heat-transfer mechanisms are important. Experimental observations of time temperature breakthrough profiles subsequent to a step change in the inlet fluid temperature have been compared with the theoretically predicted profiles in order to check the validity of the mathematical models. Critical values of the dimensionless groups defining the limiting range of applicability of the various models are presented.

NOMENCLATURE

A, surface area per unit bed volume [ft^2/ft^3] ($=3(1-p)/B$ for spheres);
B, sphere radius [ft];
C_g, gas specific heat [Btu/lb°F];
C_s, solid specific heat [Btu/lb°F];
F, fractional internal solid temperature;
F_g, fractional gas temperature;
F_o, fractional outlet gas temperature;
F_s, fractional solid temperature;
h_d, heat-transfer coefficient per unit surface area [Btu/hft^2°F];
i, the number of a length steps from the bed entrance;
K_r, dimensionless conduction parameter, $=k_s/h_dB$;
k, total number of steps across a radius, $=1/\Delta s$;
k_s, solid thermal conductivity [Btu/hft^2(°F/ft)];
L, bed length [ft];
l, distance from the bed entrance [ft];
M, constant, $=K_r\Delta z/3(\Delta s)^2$;
M_g, gas throughput per bed cross-section [lb/hft^2];
M_s, bed density [lb/ft^3];
m, number of a radial steps from the particle centre;
N, total number of steps in the bed length;
N_{so}, soakage number, $=vC_gB/k_s$;
n, number of a time steps since the step input;
p, void fraction;
r, distance from the centre of the sphere [ft];
s, dimensionless radius, $=r/B$;
T, temperature within a particle [°F];
T_g, gas temperature [°F];
T_{gi}, inlet gas temperature [°F];
T_{go}, outlet gas temperature [°F];
T_s, solid temperature [°F] (surface);
T_{si}, initial solid temperature [°F];
t, time since the introduction of the step change, [h];
u, superficial gas velocity [ft/h];

† Present address: Union Carbide Ltd., Charleston, West Virginia, U.S.A.

v, interstitial gas velocity [ft/h];
Y, dimensionless bed length parameter, $h_d AL/M_g C_g$;
y, dimensionless bed length, $H_d Al/M_g C_g$;
Z, dimensionless time parameter, $h_d A(t - L/u)M_s C_s$;
z, dimensionless time, $h_d(t - l/u)M_s C_s$;
Δs, grid radial increment;
Δy, grid length increment;
Δz, grid time increment;
ρ_s, solid density [lb/ft^3];
A_s, cross-sectional area of packing per cross-section of bed [ft^2/ft^2];
e, constant, $(2 - Y\Delta y)/(2 + Y\Delta y)$;
f, constant, $Y\Delta y/(2 + Y\Delta y)$;
K_f, dimensionless flux conduction parameter, $= k_s/h_d L$;
K_L, dimensionless longitudinal conduction parameter, $= k_s A_s/M_g C_g L$;
x, constant $\frac{1}{2}K_L\Delta y/Y(\Delta y)^2$;
[ ], Small square brackets contain the grid coordinates of the preceding temperature point F_g, F_s.

INTRODUCTION

THE SCHUMANN model [1] comprising a pair of coupled hyperbolic partial differential equations has been applied in many instances [2–10] to determine the heat transfer coefficient for a gas flowing through a fixed bed. This model, however, assumes that the thermal conductivity of the packing material does not affect the heat transfer although in many cases this is not so. This present work arose out of the need to check that heat-transfer coefficients derived [10] by use of the Schumann model were free of the effect of the packing thermal conductivity.

Mathematical models [11–17] have been proposed for the inclusion of the packing conductivity, and analytical solutions derived [13, 18, 19], although their use is cumbersome. Numerical solutions may be handled more easily provided the solution has been shown to be valid. This may be achieved by comparison with the analytical solution or by comparison with the simple solution (Schumann model) when the effect of conductivity is allowed to become small.

The models presented here are solved numerically for the particular case of a fluid flowing in one direction through a fixed bed so as to calculate the breakthrough temperature profile when the inlet fluid temperature is subjected to a step change. Analysis of the shape of the breakthrough temperature profile can be used to calculate the convective heat-transfer coefficient at the packing surface.

The same models with different boundary conditions may be used to describe the operation of a pair of reversing thermal regenerators [20–22]. Hausen [23] and Butterfield [24] have shown that for this particular case the point temperatures in the solid packing vary almost linearly with time throughout the flow cycle and an overall (lumped) heat-transfer coefficient incorporating the thermal resistance of the packing may be employed in the analytical solution of the Schumann model to calculate the thermal efficiency and temperature distributions.

Razelos and Lazaridis [40] have presented computed values of correction factors which can be used to obtain lumped heat-transfer coefficients from convective film coefficients for subsequent use in the Schumann model as applied to a simple thermal regenerator with hollow cylindrical packing geometry. This approach may, however, be inadequate when additional complications such as varying physical properties, heat-transfer coefficients and heat sources are present.

Willmott [25] has presented computer solutions for the Schumann model with boundary conditions simulating a pair of reversing thermal regenerators and these may be extended to allow for the temperature variation of physical properties and heat-transfer coefficient within the packing. Solutions of the same problem using electrical resistance analogues have been used by Hlinka [26] and Razelos [27] to investigate the design and performance of blast furnace regenerator stoves.

THE SIMPLE OR SCHUMANN MODEL

This model has received much attention in the literature [2, 4, 6, 9, 10] and thus will be dealt with briefly here. The equations describing this model when put in dimensionless form are as follows,

$$\partial F_g/\partial y = -(F_g - F_s) \tag{1}$$

and

$$\partial F_s/\partial z = +(F_g - F_s). \tag{2}$$

The following simplifying assumptions being taken:

(a) The thermal constants of the system are independent of temperature.
(b) There is no radial heat transfer.
(c) The fluid is in plug flow.
(d) Axial conduction in either the fluid phase or the solid phase is negligible.
(e) The fluid velocity does not vary along the bed.
(f) There is no thermal gradient within the particles.

Numerical solutions for this model have been derived and shown to be stable and convergent for a variety of initial and boundary conditions [9, 10, 14, 25, 28]. However the computing time for obtaining a solution depends upon the numerical method. The central difference scheme proposed by Price [9] which is identical to the trapezoidal approximation proposed by Willmott [25], would appear to be the superior one. In this case, integration step sizes of 0·3 guarantee accuracy to three decimal places. The Price solution was used as a comparison for the solutions obtained later which include the effects of packing conductivity.

INTRAPARTICLE CONDUCTION EFFECTS

For packed beds containing particles of low thermal conductivity material, e.g. glass and ceramics, assumption (f) of the simple model is invalid under certain conditions in which case allowance must be made for thermal gradients within the particles, i.e. intraparticle conduction effects.

A heat balance across an element of the bed, as shown in Fig. 1, for the fluid phase gives

$$M_g C_g \partial T_g/\partial l + (M_g C_g/u)\partial T_g/\partial t = -h_d A(T_g - T_s). \tag{3}$$

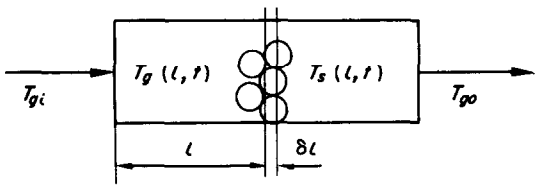

FIG. 1. Model of the packed bed.

The thermal behaviour for each particle, see Fig. 2 (assumed to be spheres of radius B), is described by

$$\rho_s C_s \partial T/\partial t = k_s(\partial^2 T/\partial r^2 + (2/r)\partial T/\partial r). \tag{4}$$

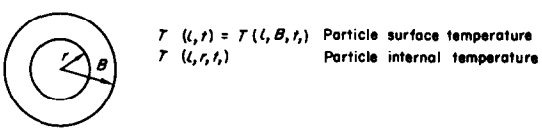

FIG. 2. Individual spherical particle.

The equations (3) and (4) are coupled by the heat balance at the gas-solid interface,

$$-k_s(\partial T/\partial r)_{r=B} = h_d(T_s - T_g) \tag{5}$$

and the system is completed by the symmetry condition

$$(\partial T/\partial r)_{r=0} = 0. \tag{6}$$

The initial and boundary conditions, representing a step change in the gas inlet temperature are

$$T_g = T_{gi} \quad \text{for} \quad l = 0 \quad \text{and} \quad t \geqslant 0, \tag{7}$$

and

$$T = T_s = T_{si} \quad \text{for} \quad t = 0, \quad B \geqslant r \geqslant 0 \quad \text{and} \quad L \geqslant l \geqslant 0. \tag{8}$$

The equations (3) through to (8) are made

dimensionless by transforming the independent variables l, t and r using the following substitutions.

$$y = h_d A l / M_g C_g, \tag{9}$$

$$z = (t - 1/u)\, h_d A / M_s C_s, \tag{10}$$

$$s = r/B \tag{11}$$

and

$$K_r = k_s / h_d B, \tag{12}$$

and introducing the normalized temperatures

$$F = (T - T_{si})/(T_{gi} - T_{si}), \tag{13}$$

$$F_g = (T_g - T_{si})/(T_{gi} - T_{si}) \tag{14}$$

and

$$F_s = (T_s - T_{si})/(T_{gi} - T_{si}). \tag{15}$$

Thus the following equations describe the intraparticle conduction model for transient heat transfer between fluid and solid in a fixed bed.

$$\partial F_g / \partial y = -(F_g - F_s), \tag{16}$$

$$\partial F / \partial z = (K_r/3)(\partial^2 F / \partial s^2 + (2/s)\, \partial F / \partial s), \tag{17}$$

$$-K_r (\partial F / \partial s)_{s=1} = +(F_g - F_s) \tag{18}$$

and

$$(\partial F / \partial s)_{s=0} = 0, \tag{19}$$

with the following initial and boundary conditions,

$$F_g = 1 \quad \text{at} \quad y = 0 \quad \text{and} \quad z \geqslant 0 \tag{20}$$

and

$$F = F_s = 0 \quad \text{at} \quad z = 0,\ 1 \geqslant s \geqslant 0 \quad \text{and} \quad Y \geqslant y \geqslant 0. \tag{21}$$

NUMERICAL SOLUTION OF THE INTRAPARTICLE CONDUCTION MODEL

The packed bed is now represented by a three dimensional grid as shown in Fig. 3.

The equation (16) is approximated by central difference formula giving

$$\frac{F_g[n+1,i] - F_g[n+1,i-1]}{\Delta y} = -\tfrac{1}{2}(F_g[n+1,i] + F_g[n+1,i-1] - F_s[n+1,i] - F_s[n+1,i-1]) + 0(\Delta y^2) \tag{22}$$

where the symbols inside the square brackets indicate the coordinates on the computational grid of the gas and solid temperatures F_s and F_g.

The equation (17) is represented by the Crank–Nicholson 6-point implicit form [29], resulting in

$$\frac{F[n+1,i,m] - F[n,i,m]}{\Delta z} = \frac{K_r}{6\Delta s^2}\Big\{(1 + 1/m)\, F[n+1,i,m+1] - 2F[n+1,i,m] + (1 - 1/m)\, F[n+1,i,m-1] + (1 + 1/m)\, F[n,i,m+1] - 2F[n,i,m] + (1 - 1/m)\, F[n,i,m-1] + 0(\Delta z) + 0(\Delta s)^2.\Big\} \tag{23}$$

The equation (18) for the gas-solid interface is approximated by central difference formula by assuming the existence of a temperature at a

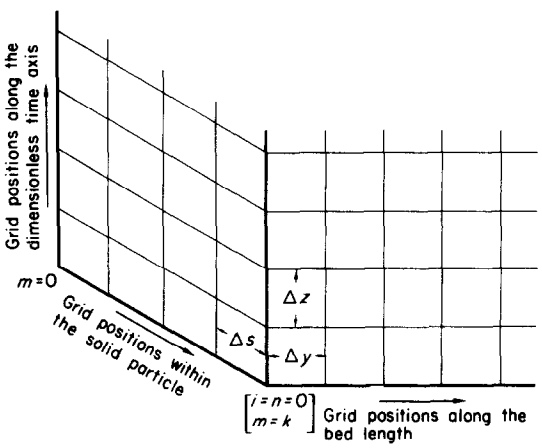

FIG. 3. Numerical grid representation of the bed.

distance Δs from the solid surface, position $(k+1)$,

$$-K_r\frac{(F[p,i,k+1]-F[p,i,k-1])}{2\Delta s} = F_s[p,i]-F_g[p,i]+0(\Delta s^2) \quad (24)$$

where $p = n, n+1$.

The truncation error in equation (24) matches that used in equation (23). The hypothetical temperatures obtained when $m = k$ in equation (23) may be eliminated by using equation (24) thus giving the following equation;

$$\begin{aligned}F[n+1,i,k]-F[n,i,k] &= M(F[n+1,i,k-\ 1]-F[n+1,i,k]\\ &+F[n,i,k-1]-F[n,i,k]\\ &+\Delta s(1+1/k)/K_r(F_g[n+1,i]\\ &-F[n+1,i,k]+F_g[n,i]-F[n,i,k])) \quad (25)\end{aligned}$$

$$M = K_r\Delta z/3\Delta s^2.$$

At the centre of the particle, $m = 0, \partial F/\partial s = 0$, and the indeterminate term $(2/s)\,\partial F/\partial s$ has the limit $2\partial^2F/\partial s^2$ at $s = 0$, so that equation (17) becomes,

$$\partial F/\partial z = K_r\partial^2F/\partial s^2 \quad \text{at} \quad s = 0. \quad (26)$$

The Crank–Nicholson representation of equation (26), and the condition of symmetry give the following equation

$$\begin{aligned}F[n+1,i,0]-F[n,i,0] &= 3M(F[n+1,i,1]-F[n+1,i,0]\\ &+F[n,i,1]-F[n,i,0]). \quad (27)\end{aligned}$$

The $(k+2)$ algebraic equations (22), (23), (25) and (27) describe the intraparticle conduction model by finite difference approximation and at the $(n+1, i)$ step point there will be $(k+2)$ unknown temperatures, $F_g[n+1,i]$ and $F[n+1,i,m=0\rightarrow k]$, provided the gas and solid temperatures at the (n, i) point, and the gas temperature at the $(n+1,\ i-1)$ point are known.

The starting values for the solution are obtained from the initial and boundary conditions, which in their finite-difference form are as follows:

$$F_g[n,i] = 1 \quad \text{at} \quad i = 0 \quad \text{and} \quad n \geqslant 0. \quad (28)$$

$$F[n,i,m] = 0 \quad \text{at} \quad n = 0, k \geqslant m \geqslant 0 \quad \text{and} \quad n \geqslant i \geqslant 0 \quad (29)$$

and

$$F_s[n,i] = F[n,i,k]. \quad (30)$$

The resulting set of algebraic equations (22), (23), (25) and (27) are represented for convenience in the matrix form by $\bar{A}\bar{x}(n+1) = \bar{B}(n)$, for a given length position, i, where $\bar{A}$ is a $(k+2)\times(k+2)$ tridiagonal matrix, $\bar{x}(n+1)$ is a $(k+2)$ column vector of the unknown temperatures and $\bar{B}(n)$ is a $(k+2)$ column vector of the known temperatures. The components of $\bar{A}, \bar{x}(n+1)$ and $\bar{B}(n)$ are shown in Appendix 1, and the solution is merely the inversion $\bar{x}(n+1) = \bar{B}(n)\,A^{-1}$, which is achieved by a Gauss elimination and substitution procedure (41), on the tridiagonal matrix.

Stability and Convergence of the Numerical Solution of the Intraparticle Conduction Model

The stability of the hyperbolic and parabolic partial differential equations are known but the manner of coupling these two equations by the flux boundary condition at the particle surface may seriously affect the overall stability of the numerical analysis. Parker and Crank [30] Albasiny [31] and Keast and Mitchell [32] have discussed the stability of the Crank–Nicholson formula for various parabolic partial differential equations and boundary conditions, and found that persistent discretization errors may occur in the solution. These errors are dependent upon the increment size used in the approximation of the parabolic equation.

The numerical analysis was initially checked for stability at the zero length condition where the system is in fact the following

$$\frac{\partial F}{\partial z} = K_r\left[\frac{\partial^2F}{\partial s^2}+\left(\frac{2}{s}\right)\frac{\partial F}{\partial s}\right] \quad (31)$$

Table 1. Stability of the zero length condition

	Δz	Δs	$z = 0{\cdot}1$ F_s	2·0 F_s	$F_s = 0{\cdot}999$ Steps	F_s
$K_r = 100$	0·01	0·20	0·09659	0·86440	693	0·99901
	0·05	0·20	0·09511	0·86420	139	0·99905
	0·10	0·20	0·09875	0·86365	69	0·99930
	0·10	0·10	0·09870	0·86352	69	0·99950
	0·10	0·05	0·09880	0·86349	69	0·99958
	0·20	0·20	0·69813	0·86367	35	0·99926
$K_r = 1{\cdot}0$	0·01	0·20	0·20179	0·84387	870	0·99937
	0·05	0·20	0·20453	0·84391	174	0·99937
	0·10	0·20	0·22435	0·84402	87	0·99937
	0·10	0·10	0·24660	0·84372	87	0·99937
	0·10	0·05	0·25536	0·84085	87	0·99938
	0·20	0·20	0·64813	0·84433	44	0·99943
$K_r = 0{\cdot}1$	0·01	0·20	0·30626	0·86740	2875	0·99990
	0·05	0·20	0·30776	0·86741	575	0·99990
	0·10	0·20	0·31267	0·86745	288	0·99990
	0·10	0·10	0·44365	0·86285	284	0·99990
	0·10	0·05	0·53995	0·86182	283	0·99990
	0·20	0·20	0·79603	0·86760	144	0·99990

and

$$K_r \left(\frac{\partial F}{\partial s}\right)_{s=1} = F_s - F_g \tag{32}$$

with $F_g = 1$ for $z \geqslant 0$ and $F_s = F = 0$ at $z = 0$ and $1 \geqslant s \geqslant 0$. Table (1) shows the values of F_s the particle surface temperature for $z = 0{\cdot}1$ and 2·0, the number of time steps required for the value of F_s to reach 0·999 and the value at that time for $\Delta z = 0{\cdot}01$, 0·05, 0·1, 0·2 and for $\Delta s = 0{\cdot}2$, 0·1, 0·05. Decreasing the size of Δz the time step only affects the value of F_s at very small values of z which is caused by the discontinuity due to the initial condition, although these effects are damped away when z has reached 2·0. The number of increments within the particle has little effect on the values of F_s until the value of K_r has decreased to 0·1. The latter value of K_r easily represents the lower limit one would expect for a physical situation whilst the solution is stable and convergent for values greater than 0·1 and shows no effect of any discretization errors.

The numerical solution was checked for overall stability and convergence by comparison with the infinite integral solution derived by Rosen [18, 19] for the analogous case of solid diffusion in packed beds. He tabulated values of $u(v, x, y)$ for various values of x, v/x and y/x which were obtained by a numerical solution. Rosen's parameters were defined as follows,

$$u(v, x, y) = C/Co, \text{fractional concentration} \tag{33}$$

$$x = 3DKz/mvb^2, \text{dimensionless length} \tag{34}$$

$$y = 2D(t - z/v)/b^2, \text{dimensionless time} \tag{35}$$

and

$$v = 3DKR_f/b^2, \text{film resistance parameter} \tag{36}$$

and the relationships between these parameters and those used in this study are

$$u = F_0 \tag{37}$$

$$v = K_r \tag{38}$$

$$x = K_r Y \tag{39}$$

and

$$y = 2K_r Z/3. \tag{40}$$

Table 2 shows the excellent agreement be-

tween Rosen's results and those obtained here, which indicates that the finite-difference scheme converges to the correct solution. This was further substantiated by comparison with the Schumann model, for large values of K_r (= 100) when the intraparticle model approaches the Schumann one and this is shown in Table 3.

The stability was tested by decreasing the step sizes, and accuracy to two decimal places was guaranteed by using the step sizes $\Delta s = \Delta y = \Delta z = 0{\cdot}2$, provided $K_r > 0{\cdot}1$.

Table 2. Comparison of Rosen's and the intraparticle model results

$c/c_0 = F_0$	y/x	Z'	Z
$y/x = 0{\cdot}2$; $Y = 5$; $x = 40$; $v = K_r = 8{\cdot}0$;			
0·049	0·10	0·75	0·75
0·117	0·20	1·50	1·51
0·252	0·35	2·66	2·63
0·454	0·55	4·13	4·13
0·675	0·80	6·00	6·00
0·849	1·10	8·25	8·25
0·992	2·00	15·00	15·01
$y/x = 0{\cdot}025$; $Y = 40$; $x = 40$; $v = K_r = 1{\cdot}0$;			
$c/c_0 = F_0$	y/x	Z'	Z
0·015	0·35	21·00	21·08
0·152	0·50	30·00	30·00
0·361	0·60	36·00	36·00
0·484	0·65	39·00	39·00
0·604	0·70	42·00	42·01
0·799	0·80	48·00	48·00
0·970	1·00	60·00	59·98
$y/x = 0{\cdot}1$; $Y = 10$; $x = 0{\cdot}5$; $v = K_r = 0{\cdot}05$;			
$c/c_0 = F_0$	y/x	Z'	Z
0·128	0·10	1·50	1·56
0·263	0·20	3·00	3·00
0·421	0·35	5·25	5·22
0·517	0·47	7·05	7·02
0·654	0·70	10·50	10·47
0·778	1·00	15·00	15·16
0·948	2·00	30·00	29·89

Z' was calculated from Rosen's results.
Z was computed using the intraparticle model employing the following step sizes.
$\Delta y = \Delta z = 0{\cdot}2$; $\Delta s = 0{\cdot}1$.

DISCUSSION OF THE INTRAPARTICLE CONDUCTION MODEL

For the Schumann model, at each value of Y a uniquely shaped breakthrough (outlet gas temperature) curve exists, a few are shown in Fig. 4. However for the intraparticle conduction model for each value of Y a family of curves exists for various values of K_r and Fig. 5 shows a range of these. As mentioned earlier as K_r increases the intraparticle model approaches the Schumann one, unfortunately no satisfactory

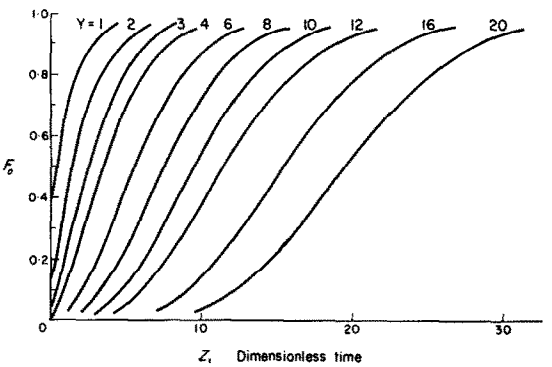

FIG. 4. Breakthrough curves for the Schumann model.

Table 3. Comparison of the intraparticle and Schumann models

	$Y = 4$		$Y = 8$		$Y = 12$	
F	Z'	Z	Z'	Z	Z'	Z
0·1	0·81	0·81	3·28	3·27	6·11	6·11
0·2	1·54	1·54	4·54	4·54	7·77	7·77
0·3	2·19	2·19	5·57	5·57	9·09	9·09
0·4	2·83	2·82	6·53	6·53	10·30	10·30
0·5	3·49	3·49	7·49	7·49	11·05	11·49
0·6	4·22	4·21	8·52	8·52	12·76	12·76
0·7	5·07	5·07	9·70	9·70	14·18	14·18
0·8	6·16	6·16	11·17	11·17	15·93	15·94
0·9	7·84	7·84	13·37	13·37	18·54	18·54

Z' Schumann model. Z intraparticle model and the step sizes employed were $\Delta s = \Delta y = \Delta z = 0{\cdot}1$.

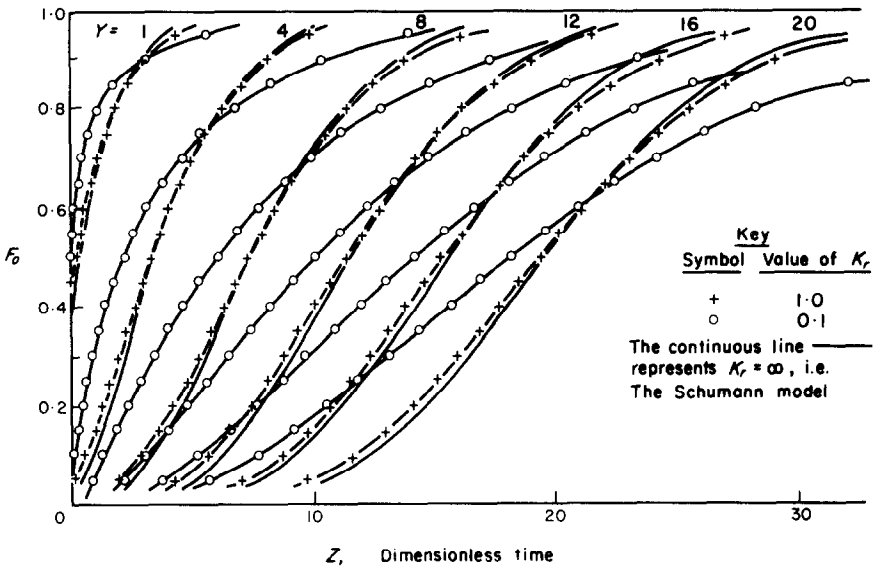

FIG. 5. Breakthrough curves for the intraparticle conduction model.

definition has been found which will predict a dividing line between the two models. Such a definition would be useful because the computing time required to obtain a solution by the intraparticle model is far in excess of that required using the Schumann model.

Saunders and Ford [33] proposed from experimental observations that provided the value of the dimensionless group, $N_{so} = vdC_g/k_s$, was less than 4 the effect of intraparticle conduction is insignificant, whereas Chukhanov and Shapatina [34] showed that the use of Schumann's model is limited to values of the inverse of the Biot number, $k_s/h_d d > 1$–1·5. These two groups differ by the terms, vC_g and h_d, and it is questionable which of the two groups gives the best prediction of the correct model.

The conduction parameter K_r is twice the inverse of the Biot number, hence on the basis of the Chukhanov and Shapatina prediction, using $K_r = 10$, the breakthrough curves for the intraparticle and Schumann models should coincide. It is evident from Table 4 that this is not so, although as the value of Y is increased

Table 4. Investigation of the Chukhanov and Shapatina prediction for $K_r = 10$

	$Y = 2$			$Y = 4$			$Y = 8$		
F_0	Z'	Z	e(%)	Z'	Z	e(%)	Z'	Z	e(%)
0·1		No value		0·817	0·791	−3·1	3·280	3·238	−1·3
0·2	0·240	0·221	−7·1	1·543	1·519	−1·2	4·539	4·504	−0·8
0·3	0·620	0·602	−2·9	2·191	2·170	−0·9	5·569	5·541	−0·5
0·4	1·024	1·009	−1·4	2·826	2·810	−0·5	6·529	6·510	−0·3
0·5	1·470	1·458	−0·8	3·488	3·477	−0·3	7·494	7·484	−0·1
0·6	1·980	1·974	−0·3	4·218	4·212	−0·1	8·524	8·524	0·0
0·7	2·599	2·600	0·0	5·065	5·017	+0·1	9·698	9·710	+0·1
0·8	3·421	3·430	+0·3	6·155	6·173	+0·3	11·166	11·194	+0·3
0·9	4·728	4·755	+0·6	7·836	7·875	+0·5	13·369	13·424	+0·4

Z' Schumann model; Z intraparticle model; $e = 100(Z - Z')/Z'$ (%).

the two curves seem to approach each other. This particular prediction concerning the limitation on the use of the Schumann model does not seem to be valid.

From the consideration of Table 4 values of Y were investigated to find those values of K_r which gave an approximate 1·0 per cent agreement between the curves for the two models at either the 0·2 or 0·8 fractional temperature points. In Table 5 the curve points at 0·1 intervals are presented for the two models at which the above agreement was obtained. The product of Y and K_r at which the stated agreement occurs is 60 and thus this value seems to predict a dividing line between the two models. Now

$$YK_r = h_d ALk_s/M_g C_g Bh_d > 60 \qquad (41)$$

or

$$YK_r = 3k_s L(1 - p)/M_g C_g B^2 > 60. \qquad (42)$$

The above dimensionless group does not contain the heat-transfer coefficient, but it does contain the bed length and the bed voidage, whereas neither of the previously proposed groups contained any of the bed properties except that they used the interstitial velocity. Hence the prediction by equation (42) infers that the shorter the bed length, the smaller the value of YK_r and hence there is a greater possibility of intraparticle conduction effects. The dimensionless group N_{so} proposed by Saunders and Ford does not have the flexibility of $YK_r > 60$.

Butterfield [24] has shown that the use of an overall coefficient of the type proposed by Hausen [35] in the Schumann model equations of a reversing regenerator may lead to significant errors particularly when the reversing period is short. It is therefore important when seeking a correct numerical simulation of a reversing thermal regenerator that the intra particle conduction test be applied before selecting the appropriate mathematical model.

Table 5. Comparison of the Schumann and intraparticle models

	$Y = 4$ $K_r = 15$			$Y = 12$ $K_r = 5$			$Y = 20$ $K_r = 3$		
F_0	Z'	Z	e(%)	Z'	Z	e(%)	Z'	Z	e(%)
0·1	0·817	0·800	−1·7	6·112	6·106	−1·7	12·271	12·034	−1·9
0·2	1·543	1·519	−0·9	7·773	7·689	−1·1	14·561	14·386	−1·2
0·3	2·191	2·177	−0·6	9·093	9·029	−0·7	16·333	16·210	−0·7
0·4	2·826	2·815	−0·3	10·301	10·258	−0·4	17·929	17·855	−0·4
0·5	3·408	3·481	−0·2	11·496	11·458	−0·2	19·489	19·464	−0·1
0·6	4·215	4·213	−0·1	12·757	12·761	0·0	21·114	21·141	+0·1
0·7	5·065	5·069	+0·1	14·177	14·211	+0·2	22·925	23·012	+0·4
0·8	6·155	6·168	+0·2	15·933	16·005	+0·5	25·141	25·302	+0·6
0·9	7·833	7·862	+0·3	18·535	18·667	+0·7	28·385	28·656	+1·0

Z' Schumann model; Z intraparticle model; $e = 100(Z - Z')/Z'$%.

EXPERIMENTAL TEST OF THE INTRAPARTICLE CONDUCTION MODEL

The experimental apparatus and procedure are described elsewhere [10, 36]. To test the model it is necessary to show that the experimental observations and simulating calculations have identical breakthrough curves and this was attempted over a wide range of conditions, two cases of which are presented here.

The characteristic data for the two fixed beds and the operating conditions are shown in Table 6.

The convective heat-transfer coefficients were obtained from a correlation presented by the authors for results obtained solely for metallic spheres [36]. Figures 6 and 7 show the com-

Table 6. Characteristic data for the two fixed beds

Bed no.	1	2
Bed length, in.	6·12	8·17
Bed diameter, in.	2·74	2·73
Packing material	Lead	Soda glass
Packing size, in.	0·357	0·238
Packing specific gravity.	11·35	2·51
Packing specific heat, Btu/lb°F.	0·03	0·189
Gas specific heat, Btu/lb°F.	0·24	0·24
Bed density, lb/ft^3.	443·7	99·1
Bed voidage.%	37	37
Gas mass throughput, lb/h ft^2.	5564	5623
Superficial velocity, ft/sec.	19·26	19·60
Convective heat-transfer coefficient Btu/hft^2 °F.	69·5	83·5
Specific surface, ft^2/ft^3.	120	181
Thermal conductivity of material, Btu/hft^2 (°F/ft).	20	0·60

parisons and there is excellent agreement between the shapes of the curves although they do not coincide. This difference between the predicted and experimental curves was due to the slight tailing of the step input which was not completely square. The step increments used in the computation were $\Delta z = \Delta y = 0{\cdot}2$ and $\Delta s = 0{\cdot}1$.

Table 7 shows the comparison between the curve points predicted for these runs both for the Schumann case and the intraparticle case. Very good agreement is obtained for run 1, where lead shot were used as the packing, but for run 2 the curves differ considerably. The value of YK_r for run 1 was 66·2 whilst that for run 2 was 6·1. Hence for run 2 considerable

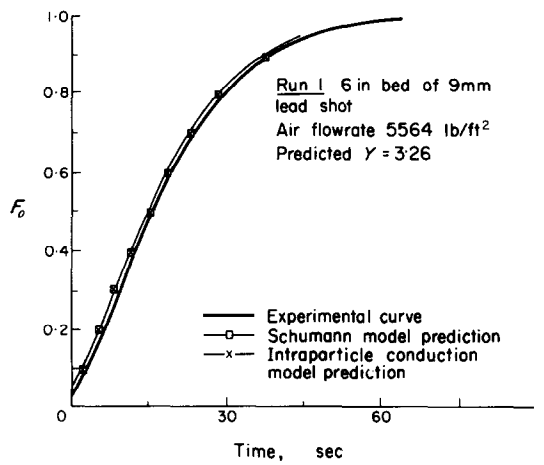

FIG. 6. Breakthrough curve comparison for run 1.

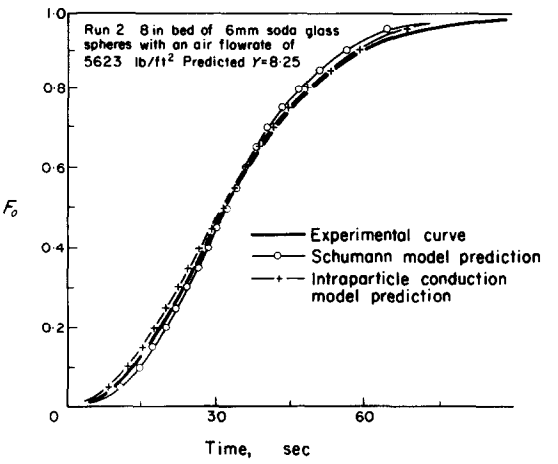

FIG. 7. Breakthrough curve comparison for run 2.

Table 7. Curve points predicted by the Schumann and intraparticle conduction models

	Run 1		Run 2		
F_0	t' (sec)	t (sec)	t' (sec)	t (sec)	
$Y = 3{\cdot}26$,	$K_r = 20{\cdot}23$,	$YK_r = 66{\cdot}2$	$Y = 8{\cdot}25$,	$K_r = 0{\cdot}74$, $YK_r = 6{\cdot}1$	
0·1	2·47	2·40	14·22	12·10	
0·2	5·85	5·78	19·52	17·68	
0·3	8·98	8·91	23·85	22·36	
0·4	12·11	12·05	27·87	26·79	
0·5	15·41	15·38	31·94	31·29	t' Schumann model
0·6	19·09	19·07	36·22	36·14	t intraparticle model
0·7	23·42	23·45	41·13	41·71	
0·8	29·04	29·10	47·25	48·73	
0·9	37·79	37·90	56·45	59·36	

intraparticle conduction effects are present, whilst run 1 is free of them.

The intraparticle conduction model fits the experimental one extremely well, which indicates that the breakthrough curve for beds where intraparticle conduction effects are present, may be predicted accurately using this model. It is important however to check firstly that intraparticle effects will be encountered, because otherwise the Schumann model may be used for the prediction thus saving considerable computing time. The excellent predictions obtained here infer that the heat-transfer coefficients used were in fact the convective ones. Hence the results presented earlier for metallic spheres were free of the effects of intraparticle conduction, whilst the results for the non-metallic spheres were affected under certain flow conditions.

THE EFFECT OF AXIAL CONDUCTION IN THE SOLID

If the packing is not particulate, but in the form of material parallel to the fluid flow, assumption (*d*) for the Schumann model will only be partially valid, because there may be axial conduction of heat in the solid phase. The packing is now assumed to be continuous lengths L equal to that of the packed bed and heat balance equations may again be formulated. The one for the fluid phase is unchanged, i.e.

$$M_g C_g \partial T_g/\partial l + (M_g C_g/u)\,\partial T_g/\partial t = -h_d A(T_g - T_s) \qquad (43)$$

whilst the one for the solid phase is

$$M_s C_s \partial T_s/\partial t = h_d A(T_g - T_s) + k_s A_s \partial^2 T_s/\partial l^2. \qquad (44)$$

The initial and boundary conditions which again represent a step change in the gas inlet temperature are

$$T_g = T_{gi} \quad \text{for} \quad l = 0 \quad \text{and} \quad t \geqslant 0 \qquad (45)$$

and

$$T_s = T_{si} \quad \text{for} \quad t = 0 \quad \text{and} \quad L \geqslant l \geqslant 0. \qquad (46)$$

Additional boundary conditions must be considered to solve (44) at the extremities of the beds and two types of conditions may be assumed.

1. Adiabatic boundary conditions

$$\partial T_s/\partial l = 0 \quad \text{at } l = 0 \quad \text{and} \quad l = L \quad \text{for} \quad t \geqslant 0. \qquad (47)$$

2. Flux boundary conditions,

$$-k_s \partial T_s/\partial l = h_d(T_g - T_s) \quad \text{at} \quad l = 0$$

and

$$l = L \quad \text{for} \quad t \geqslant 0. \qquad (48)$$

Equations (3) and (44) through (48) are made dimensionless by transforming the independent variables l and t by the substitutions,

$$z = (t - l/u)\, h_d A/M_s C_s \qquad (10)$$

$$y = l/L \qquad (49)$$

$$Y = h_d AL/M_g C_g \qquad (50)$$

$$K_L = k_s A_s/M_g C_g L \qquad (51)$$

and

$$K_f = k_s/h_d L, \qquad (52)$$

and the introduction of the normalized temperatures

$$F_g = (T_g - T_{si})/(T_{gi} - T_{si}) \qquad (14)$$

and

$$F_s = (T_s - T_{si})/(T_{gi} - T_{si}). \qquad (15)$$

Hence the equations

$$\partial F_g/\partial y = -Y(F_g - F_s) \qquad (53)$$

$$\partial F_s/\partial z = (F_g - F_s) + (K_L/Y)\,\partial^2 F_s/\partial y^2 \qquad (54)$$

with the following initial and boundary conditions,

$$F_g = 1 \quad \text{for} \quad y = 0 \quad \text{and} \quad z \geqslant 0, \tag{55}$$

$$F_s = 0 \quad \text{for} \quad z = 0 \quad \text{and} \quad 1 \geqslant y \geqslant 0 \tag{56}$$

and

1. Adiabatic boundary conditions,

$$\partial F_s/\partial y = 0 \quad \text{for} \quad y = 0 \quad \text{and} \quad y = 1, \quad \text{and} \quad z \geqslant 0, \tag{57}$$

2. Flux boundary conditions,

$$-K_f \partial F_s/\partial y = h_d(F_g - F_s) \quad \text{for} \quad y = 0 \quad \text{and} \quad y = 1, \quad \text{and} \quad z \geqslant 0, \tag{58}$$

describe the axial conduction model.

NUMERICAL SOLUTION OF THE AXIAL CONDUCTION MODEL

The packed bed is now represented by a grid as shown in Fig. 8. Equation (53) is approximated by central differences representation to give

$$\frac{F_g[n, i+1] - F_g[n, i]}{\Delta y} = -\tfrac{1}{2}Y(F_g[n, i+1] + F_g[n, i] - F_s[n, i+1] - F_s[n, i]) + 0(\Delta y^2). \tag{59}$$

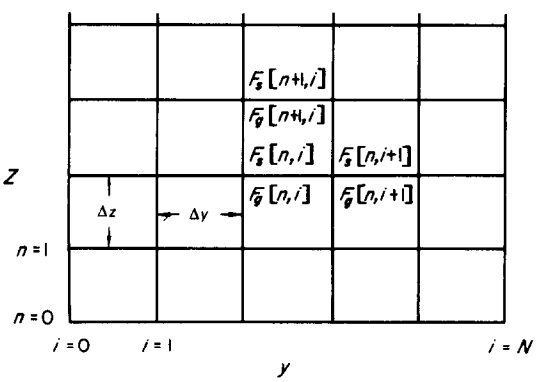

FIG. 8. Numerical grid representation.

The Crank–Nicholson representation of equation (54) is

$$F_s[n+1, i] - F_s[n, i] = +\tfrac{1}{2}\Delta z(F_g[n+1, i] + F_g[n, i] - F_s[n+1, i] - F_s[n, i]) + X\{F_s[n+1, i-1] - 2F_s[n+1, i] + F_s[n+1, i+1] + F_s[n, i-1] - 2F_s[n, i] + F_s[n, i+1]\} + 0(\Delta y^2) + 0(\Delta z) \tag{60}$$

where $X = \frac{1}{2}K_L\Delta z/Y(\Delta y)^2$. Now at the extremities of the bed, $i = 0$ and $i = N$, it is found that equation (60) includes fictitious temperatures outside the grid at the positions $i = -1$ and $i = N + 1$. Either of the boundary conditions (57) and (58) may be used to eliminate these temperatures.

The adiabatic boundary (57) is interpreted in finite difference form by assuming the existence of a temperature point a distance equal to a length step Δy outside the grid at which $F_s[-1] = F_s[0]$, hence at $i = 0$ equation (60) becomes

$$F_s[n+1, 0] - F_s[n, 0] = \tfrac{1}{2}\Delta z(F_g[n+1, 0] + F_g[n, 0] - F_s[n+1, 0] - F_s[n, 0]) + X(F_s[n+1, 1] - F_s[n+1, 0] + F_s[n, 1] - F_s[n, 0]) \tag{61}$$

and similarly at $i = N$ the assumption is that $F_s[N+1] = F_s[N]$ resulting in equation (60) becoming

$$F_s[n+1, N] - F_s[n, N] = +\tfrac{1}{2}\Delta z(F_g[n+1, N] + F_g[n, N] - F_s[n+1, N] - F_s[n, N]) + X(F_s[n+1, N-1] - F_s[n+1, N] + F_s[n, N-1] - F_s[n, N]). \tag{62}$$

The equations (60), (61) and (62) form a set of $(N+1)$ algebraic equations, but with $2(N+1) - 1$ unknowns, that is $F_g[n+1, i = 1 \to N]$ and $F_s[n+1, i = 0 \to N]$ provided the gas and solid temperatures are known at the n time step, hence these equations cannot be solved as they stand.

Now replacing n by $n+1$ in equation (59), rearranging and putting $i = 0$ we obtain

$$F_g[n+1, 1] = e + f(F_s[n+1, 1] + F_s[n+1, 0]) \tag{63}$$

where

$$e = (2 - Y\Delta y)/(2 + Y\Delta y) \tag{64}$$

and

$$f = Y\Delta y/(2 + Y\Delta y), \tag{65}$$

and the unknown gas temperature at $i = 1$ is represented by the unknown solid temperatures at $i = 0$ and $i = 1$. For $i = 1$, equation (59) becomes

$$F_g[n+1,2] = eF_g[n+1,1] + f(F_s[n+1,2] + F_s[n+1,1]) \tag{66}$$

and substitution of equation (63) in (66) gives

$$F_g[n+1,2] = e^2 + f(F_s[n+1,2] + (e+1)F_s[n+1,1] + eF_s[n+1,0]) \tag{67}$$

where the unknown gas temperature at $i = 2$ is now represented by the unknown solid temperatures at $i = 0$, 1 and 2.

Hence for the $(n + 1)$ time step the gas temperatures can be found in terms of the solid temperatures and for $i = N$, the gas temperature is given by

$$\begin{aligned} F_g[n+1,N] = {} & e^N + e^{N-1}fF_s[n+1,0] \\ & + e^{N-2}f(e+1)F_s[n+1,1] \\ & + e^{N-3}f(e+1)F_s[n+1,2] + \ldots \\ & + ef(e+1)F_s[n+1,N-2] \\ & + f(e+1)F_s[n+1,N-1] \\ & + fF_s[n+1,N]. \end{aligned} \tag{68}$$

The equations of the type (63), (67) and (68) may be substituted into equations (60), (61) and (62) to give a set of $(N + 1)$ algebraic equations of $(N + 1)$ unknown solid temperatures, $F_s[n+1, i = 0 \rightarrow N]$, which will be represented by $\bar{C}\bar{x}(n+1) = \bar{D}(n)$, where $\bar{C}$ is a $(N+1) \times (N+1)$ tri-diagonal matrix superimposed upon a $(N+1) \times (N+1)$ lower triangular matrix, $\bar{x}(n+1)$ is a $(N+1)$ column vector of the unknowns and $\bar{D}(n)$ is a $(N+1)$ column vector of the knowns. The values of unknowns in x are obtained by the inversion $\bar{x}(n+1) = \bar{D}(n)\,\bar{C}^{-1}$, this was achieved by a special back elimination and forward substitution procedure (10). The components of $\bar{C}$, $\bar{x}(n+1)$ and $\bar{D}(n)$ may be found in Appendix 2.

The flux boundary condition (58) is approximated by backward difference at $i = 0$ to give

$$-K_f\frac{(F_s[0] - F_s[-1])}{\Delta y} = (F_g - F_s[0]) + 0(\Delta y) \tag{69}$$

and by forward difference at $i = N$ to give

$$+K_f\frac{(F_s[N+1] - F_s[N])}{\Delta y} = (F_g - F_s[N]) + 0(\Delta y). \tag{70}$$

Equations (69) and (70) are used to eliminate the fictitious temperatures $F_s[-1]$ and $F_s[N+1]$ obtained in equation (60) for $i = 0$ and $i = N$. The equations of the type (63), (67) and (68) may now be used to eliminate the gas temperatures at the $(n + 1)$ time step and the resulting set of $(N + 1)$ algebraic equations with $(N + 1)$ unknown solid temperatures, represented for convenience by $\bar{C}'\bar{x}(n+1) = \bar{D}'(n)$, are solved in the identical manner as for the adiabatic boundary condition case. The components of $\bar{C}'$ and $\bar{D}'(n)$ may also be found in Appendix 2.

In both cases the values of F_g at the $(n + 1)$ time step are derived from equation (59) after the values of F_s at that time step have been evaluated. The numerical analysis is initiated by use of the initial and boundary conditions (55) and (56), which in finite-difference form are,

$$F_g[n,i] = 1 \quad \text{for} \quad i = 0 \quad \text{and} \quad n \geqslant 0 \tag{71}$$

and

$$F_s[n,i] = 0 \quad \text{for} \quad n = 0 \quad \text{and} \quad N \geqslant i \geqslant 0. \tag{72}$$

Equations (72) and (59) combine to enable the values of F_g to be evaluated at the zero time condition by the following equation,

$$F_g[0,i+1] = eF_g[0,i]. \tag{73}$$

STABILITY AND CONVERGENCE OF THE NUMERICAL SOLUTION OF THE AXIAL CONDUCTION MODEL

No analytical solution was found for this model in the literature, although Creswick [37] has derived an explicit finite-difference solution for the case of adiabatic boundaries. His solution however contains a severe stability criterion.

$$\Delta z < Y(\Delta y)^2/(2K_L + Y(\Delta y)^2) \quad (74)$$

which tends to prohibit its use, and it also appears to contain a misrepresentation in the numerical analysis. In his analysis he eliminates the fictitious temperatures outside the grid in the identical manner, as was reported for equations (61) and (62). He then continues to represent the expression $\partial^2 F_s/\partial y^2$ at the next length step $i = 1$, by (subscripts refer to values of i)

$$(\partial^2 F_s/\partial y^2)_1 = ((\Delta F_s/\Delta y)_2 - (\Delta F_s/\Delta y)_0)/2\Delta y \quad (75)$$

and states that

$$(\Delta F_s/\Delta y)_0 = 0, \quad \text{and}$$
$$(\Delta F_s/\Delta y)_2 = (F_s[3] - F_s[1])/2\Delta y$$

resulting in the following,

$$(\partial^2 F_s/\partial y^2)_1 = (F_s[3] - F_s[1])/4(\Delta y)^2. \quad (76)$$

This representation of $(\partial^2 F_s/\partial y^2)_1$, and $(\Delta F_s/\Delta y)_2$ is by central-difference approximation, and representation of $(\Delta F_s/\Delta y)_1$ in this manner gives $(F_s[1] - F_s[-1])/2\Delta y$, which by the earlier assumption cannot be zero. This assumption of $(\Delta F_s/\Delta y)_0 = 0$ implies thermal symmetry at the boundary and physically this is not so. This misrepresentation is applied at the last but one grid point. The representation of $(\partial^2 F_s/\partial y^2)_1$ would be expected to be

$$(F_s[0] - 2F_s[1] + F_s[2])/2(\Delta y)^2, \quad (77)$$

which does not alter the stability criterion.

The stability and convergence were checked by decreasing the values of Δz and Δy, and the solution was found to be more sensitive to the values of Δz. To ensure convergence to two places of decimals the value of Δz was 0·1 whilst that for Δy was 0·05, except for Y values less than 5 when 0·1 was sufficient.

The solution was checked to converge to the correct values by comparison with the Schumann case for decreasing values of K_L, when the axial conduction model approached the Schumann one. Table 8 shows this comparison and it is apparent that the Schumann model is approached as K_L is decreased.

For the flux boundary conditions, the stability was ensured provided $\Delta z \leqslant 0{\cdot}01$. This difference in the stability of the two solutions is caused by the mismatching of the truncation errors in equations (69) and (70) with those in (60). For large values of K_f the flux boundary case approaches the adiabatic one, and this was found to be true for $K_f > 10$ with $Y = 2$.

DISCUSSION OF THE AXIAL CONDUCTION MODEL

For the adiabatic boundary case, a family of curves for various values of K_L exists for each value of Y, as shown in Fig. 9, whereas for the flux boundary case, a family of curves for various values of K_f exists for each combination of Y and K_L.

No relationship that would predict a dividing line between the Schumann model and the axial conduction one has been proposed [7, 8], although for values of Y greater than 4, the product of YK_L being less than 0·1 seems to infer that the Schumann model has been reached. This relationship was obtained by a parametric investigation of the adiabatic boundary case and Table 9 shows the comparison between the Schumann and axial conduction models. Now

$$YK_L = h_d A K_s A_s/(M_g C_g)^2 < 0{\cdot}1 \quad (78)$$

and this dimensionless group contains the heat transfer coefficient but not the bed length. For Y values less than 4 the YK_L values predicting the dividing line increase in an irregular manner such that for $Y = 1$ there is good agreement between the models at $YK_L = 10$.

Table 10 presents a comparison between the Creswick and the adiabatic boundary case

Table 8. Convergence check for the axial conduction model with adiabatic boundaries

	F_0	Z'	$K_L = 0{\cdot}0$ Z	0·001 Z	0·01 Z	0·1 Z
$Y = 2$	0·1			No value		
	0·2	0·240	0·242	0·242	0·242	0·238
	0·3	0·620	0·621	0·621	0·619	0·601
	0·4	1·024	1·025	1·024	1·020	0·984
	0·5	1·470	1·469	1·469	1·462	1·408
	0·6	1·980	1·980	1·978	1·969	1·901
	0·7	2·599	2·598	2·597	2·586	2·511
	0·8	3·420	3·418	3·417	3·407	3·344
	0·9	4·728	4·276	4·726	4·726	4·733
$Y = 8$	0·1	3·280	3·288	3·281	3·221	2·770
	0·2	4·539	4·542	4·533	4·455	3·884
	0·3	5·569	5·568	5·558	5·474	4·855
	0·4	6·529	6·526	6·516	6·432	5·816
	0·5	7·494	7·489	7·480	7·403	6·839
	0·6	8·524	8·518	8·511	8·450	7·997
	0·7	9·698	9·691	9·688	9·656	9·402
	0·8	11·166	11·160	11·163	11·184	11·286
	0·9	13·369	13·368	13·385	13·524	14·380
$Y = 16$	0·1	9·132	9·160	9·128	8·856	7·010
	0·2	11·133	11·135	11·103	10·827	8·928
	0·3	12·694	12·684	12·654	12·396	10·587
	0·4	14·109	14·089	14·064	13·840	12·222
	0·5	15·498	15·473	15·453	15·280	13·933
	0·6	16·951	16·924	16·913	16·810	15·903
	0·7	18·577	18·552	18·553	18·551	18·258
	0·8	20·575	20·557	20·577	20·733	21·403
	0·9	23·513	23·517	23·573	24·028	26·538

Z' corresponds to the Schumann model.

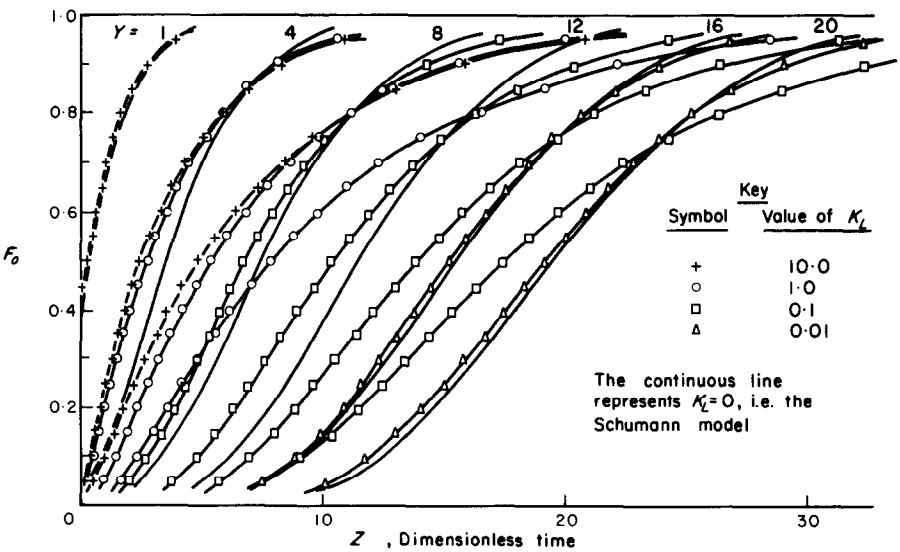

FIG. 9. Breakthrough curves for the longitudinal conduction model with adiabatic boundary conditions.

Table 9. Comparison of the Schumann and axial conduction models

	$Y = 4$ $K_L = 0{\cdot}05$			$Y = 10$ $K_L = 0{\cdot}01$			$Y = 40$ $K_L = 0{\cdot}0025$		
F_0	Z'	Z	$e(\%)$	Z'	Z	$e(\%)$	Z'	Z	$e(\%)$
0·1	0·826	0·810	−1·9	4·678	4·564	−2·4	29·050	28·635	−1·4
0·2	1·548	1·511	−2·4	6·140	6·007	−2·2	32·345	32·000	−1·1
0·3	2·192	2·138	−2·5	7·317	7·179	−1·9	34·872	34·597	−0·8
0·4	2·825	2·758	−2·4	8·403	8·273	−1·6	37·134	36·933	−0·5
0·5	3·484	3·410	−2·1	9·487	9·374	−1·2	39·336	39·218	−0·3
0·6	4·209	4·135	−1·8	10·636	10·554	−0·8	41·623	41·603	0·0
0·7	5·058	4·996	−1·2	11·939	11·907	−0·2	44·165	44·268	+0·2
0·8	6·148	6·122	−0·4	13·561	13·614	+0·4	47·269	47·540	+0·6
0·9	7·832	7·908	+1·0	15·981	16·215	+2·1	51·805	52·361	+0·9

Z' Schumann model; Z longitudinal model; $e = 100\,(Z - Z')/Z'\%$.

Table 10. Comparison of Creswick's solution

				Creswick				
			$F_0=$	0·1	0·2	0·5	0·8	0·9
Y	K_L	Δz	Δy	Z	Z	Z	Z	Z
8	0·1	0·004	0·01	2·773	3·897	6·902	11·450	14·629
8	1·0	0·010	0·05	1·588	2·519	5·450	12·566	14·575
16	0·1	0·031	0·02	7·091	9·056	14·244	21·949	27·290
16	1·0	0·019	0·05	3·669	5·609	12·851	26·885	37·484
				This work				
8	0·1	0·10	0·05	2·770	3·884	6·839	11·286	14·380
8	1·0	0·10	0·05	1·527	2·380	5·438	11·312	15·755
16	0·1	0·10	0·05	7·010	8·927	13·953	21·403	26·538
16	1·0	0·10	0·05	3·206	4·739	10·162	20·522	28·357

solutions. The Creswick solution predicts much shallower curves and the difference between the solutions becomes greater as K_L increases. The Crank–Nicholson implicit scheme employs much larger time steps than the explicit scheme and saves a considerable amount of computing time.

It is interesting to note that the simple criteria used by Tipler [38] to test for the importance of axial conduction in the solid is equivalent to K_L and therefore

$$K_L = \frac{\text{Axial heat flux in the solid}}{\text{Heat flux from fluid to solid over total bed.}}$$

The criteria for axial conduction defined here differs from the above in that it is calculated on the basis of a single transfer unit and is therefore independent of bed length.

$$YK_L = \frac{\text{Axial heat flux in solid}}{\text{Heat flux from fluid to solid per unit dimensionless bed length.}}$$

Hlinka and Landau [39] have also considered the effects of longitudinal conduction in the tube wall on the performance and temperature distribution in a steady state counterflow heat exchanger, however their analytical treatment is applicable only to the case of reversing thermal regenerators operating at short cycle times.

EXPERIMENTAL TEST OF THE AXIAL CONDUCTION MODEL

The apparatus and experimental procedure are described elsewhere [36] and the packings

employed consisted of $\frac{1}{8}$ in. thick aluminium plate sets of various lengths and spacings. Hence the packing material was not continuous along the bed length thus the physical situation is not analogous to the theoretical model presented here. The physical model was simulated theoretically by considering each plate set to be a separate bed and the overall test bed a series of these separate beds. The zero length conditions for the sets after the first one is that the F_g at the entrance to the set is taken as the exit temperature from the previous set.

The characteristic data and operating conditions for two fixed beds are shown in Table 11. The heat-transfer coefficients were obtained from measurements taken by the authors [36], where the Schumann model was assumed to fit the physical model.

Table 11. Characteristic data for the two fixed beds

Bed no.	3	4
Bed Length in.	8·12	8·13
Bed Diameter in.	2·74	2·72
Packing material.	Aluminium	Aluminium
Material thickness, in.	$\frac{1}{8}$	$\frac{1}{8}$
Plate spacing, in.	0·104	0·052
Plate length, in.	2	1
Packing specific gravity.	2·85	2·80
Packing specific heat, Btu/lb°F.	0·22	0·22
Gas specific heat, Btu/lb°F.	0·24	0·24
Bed density, lb/ft^3.	96·6	120·3
Bed voidage, %.	46	31
Packing characteristic dimension, in.	0·42	0·39
Gas mass throughout, lb/hft^2.	1680	5667
Superficial velocity, ft/s.	5·84	19·70
Convective heat-transfer coefficient, Btu/hft^2°F.	15·5	59·2
Specific surface, ft^2/ft^3.	94	127
Thermal conductivity of the material, Btu/hft^2(°F/ft).	127	127

The comparisons between the recorded observations and the simulated values are shown in Figs. 10 and 11, excellent agreement being obtained. The step increments used in the computation were $\Delta z = 0{\cdot}1$ and $\Delta y = 0{\cdot}05$, Table 12 shows the comparison between the curve points predicted for these runs both for the Schumann case and the axial conduction case. The good agreement infers that the physical model is free of the effects of axial conduction in the packing and thus the heat transfer coefficients reported earlier were the convective ones. For these physical conditions the Schumann model may be employed to predict the breakthrough curves hence saving computing time.

Figure 10 for run 3 also shows the predicted curve for the model which allows for a continuous packing material. The disagreement between the curve shapes indicates that this model is invalid for this bed arrangement. The values of Y are less than 4, and so the equation (78) cannot be applied to the experimental conditions to predict the effect of longitudinal conduction.

CONCLUSIONS

1. The model for the transient transfer of heat in a packed bed of spheres with allowance for intraparticle conduction effects is solved numerically by applying the Crank–Nicholson approximation to the partial differential equations. This solution is shown to converge to the correct solution by comparison with the analytical solution derived by Rosen and with the Schumann model.

2. A parametric investigation of the model

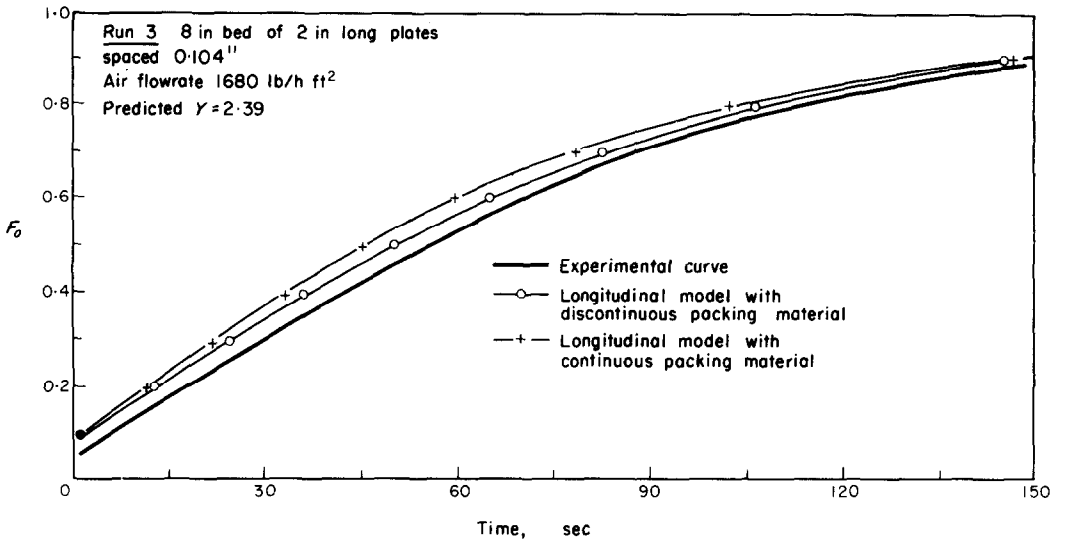

FIG. 10. Breakthrough curve comparison for run 3.

revealed a dimensionless group which predicts the dividing line between the Schumann and intra-particle conduction models. This group is independent of the convective heat-transfer coefficient, but includes the bed length and voidage. The group is shown to be superior to those predicted by Saunders and Ford, and by Chukanov and Shapatina.

3. The model predicts breakthrough curves that agree extremely well with experimental observations, whether intraparticle conduction effects are present or not.

4. The heat-transfer coefficient correlation presented elsewhere [36] by the authors for results obtained from beds of metallic spheres are confirmed by this study to be free of the

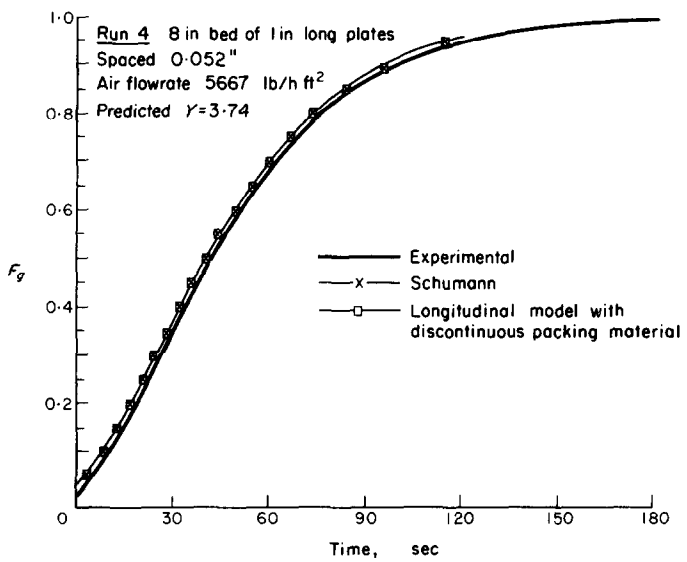

FIG. 11. Breakthrough curve comparison for run 4.

Table 12. Predicted curve points for the runs by both the Schumann and axial models

	Run 3		Run 4	
F_0	Time′ (sec)	Time (sec)	Time′ (sec)	Time (sec)
0·1	2·39	2·06	8·79	8·62
0·2	26·04	25·17	17·63	17·34
0·3	49·45	48·19	25·60	25·25
0·4	73·85	72·32	33·47	33·08
0·5	100·23	98·63	41·70	41·31
0·6	130·08	128·60	50·79	50·40
0·7	166·12	164·80	61·44	61·09
0·8	213·26	212·59	75·13	74·88
0·9	287·77	288·64	96·31	96·29

$Y = 2{\cdot}39$ $Y_B = 0{\cdot}60$ $K_{LB} = 4{\cdot}08$ $Y = 3{\cdot}74$ $Y_B = 0{\cdot}47$ $K_{LB} = 6{\cdot}08$.
Time′: Schumann model. Time: Axial conduction model.
Y: Bed length parameter. Y_B and K_{LB} refer to the individual beds within the overall bed.

effects of intraparticle conduction and are therefore convective coefficients.

5. The model for the transient transfer of heat in a bed of parallel plates with allowance for axial conduction effects in the packing material is solved numerically employing Crank–Nicholson approximations. Adiabatic and flux boundary conditions are assumed.

6. The solution for adiabatic boundaries predicts different results to those obtained by Creswick's solution which appears to contain a misrepresentation.

7. A parametric investigation revealed a dimensionless group which predicts a dividing line between the Schumann model and the axial conduction model for Y values greater than 4.

8. The model predicts breakthrough curves which agree well with experimental observations, inferring that the heat-transfer coefficients recorded previously were free of axial conduction effects.

REFERENCES

1. T. E. W. SCHUMANN, Heat transfer: A liquid flowing through a porous prism, *J. Franklin Inst.* **208**, 405 (1929).
2. C. C. FURNAS, Heat transfer from a gas stream to a bed of broken solids, *Ind. Engng Chem.* **22**, 721 (1930).
3. G. O. G. LOF and R. W. HAWLEY, Unsteady state heat transfer between air and loose solids, *Ind. Engng Chem.* **40**, 1061 (1948).
4. J. E. JOHNSON, Regenerator heat exchangers for gas turbines, *A.R.C. Tech. Rept.*, R and M No. 2630 (1948).
5. R. J. BAYLEY and C. RAPLEY, Heat transfer and pressure drop characteristics of matrices for regenerative heat exchangers, *ASME-AIChE Heat Transfer Conference, Los Angeles* (1965).
6. G. L. LOCKE, Heat transfer and flow friction characteristics of porous solids, *Tech. Rep.* No. 10 Dept. Mech. Eng., Stanford University, California (1950).
7. J. R. MONDT, Effects of longitudinal thermal conduction in the solid on apparent convection behaviour with data for plate fin surfaces, *International Developments in Heat Transfer, Boulder Conference*, 614 (1961).
8. C. P. HOWARD, Heat transfer and flow friction characteristics of skewed passages and glass ceramic heat transfer surfaces, *A.S.M.E. Paper* No. 63-WA-115.
9. C. B. A. PRICE, Heat and momentum transfer in thermal regenerators, University of London, Ph.D. Thesis (1964).
10. P. J. HEGGS, Transfer processes in packings used in regenerators, University of Leeds, Ph. D. thesis (1967).
11. W. NUSSELT, Der beharrungszustand im winderhitzen (The inertial conditioning in the heating of blast air), *Z. Ver. Dtsch. Ing.* **72**, 1052 (1928).
12. N. R. AMUNDSEN, Solid Fluid interactions in fixed and moving beds, *Ind. Engng Chem.* **48**, 26 (1956).
13. N. R. AMUNDSEN, Solid fluid interactions in fixed and moving beds, *Ind. Engng Chem.* **48**, 35 (1956).
14. P. K. LEUNG and D. QUON, A computer model of the regenerative bed, *Can. J. Chem. Engng* **44**, 26 (1966).
15. P. K. LEUNG and D. QUON, A computer model of moving beds, chemical reaction in the fluid phase only, *Can. J. Chem. Engng* **43**, 45 (1965).
16. F. T. HUNG and R. G. NEVINS, Unsteady state heat transfers with a fluid flowing through porous solids, *ASME Paper* No. 65-HT-10.
17. A. KARDAS, On a problem in the theory of the uni-

directional regenerator, *Int. J. Heat Mass Transfer* **9**, 567 (1966).
18. J. B. ROSEN, Kinetics of a fixed bed system for solid diffusion in spherical particles, *J. Chem. Phys.* **20**, 387 (1952).
19. J. B. ROSEN, General numerical solution for solid diffusion in fixed beds, *Ind. Engng Chem.* **46**, 1590 (1954).
20. H. HAUSEN, Über die theorie des warmeaustausches in regeneratoren, *Z. Angew. Math. Mech.* **9**, 173 (1929).
21. A. ANZELIUS, Über erwarmung vermittals durchströmender medien, *Z. Angew. Math. Mech.* **6**, 291 (1926).
22. C. E. ILIFFE, Thermal analysis of the contra flow regenerative heat exchanger, *Proc. Inst. Mech. Engnrs* **159**, 363 (1948).
23. H. HAUSEN, Vervollständigte berechnung des warmeaustausches in regeneratoren, *Z. Ver. Dtsch. Ing.-Beiheft Veftk.* **2**, 43 (1942).
24. P. BUTTERFIELD, J. SCHOFIELD and P. A. YOUNG, Hot blast stoves, *J. Iron Steel Inst.* **201**, 497 (1963).
25. A. J. WILLMOTT, Simulation of a thermal regenerator under conditions of variable mass flow, *Int. J. Heat Mass Transfer* **11**, 1105 (1968).
26. J. W. HLINKA, F. S. PUHR and V. PASCHKIS, AISE Manual for thermal design of regenerators, *Iron Steel Engnr*, 59 (1961).
27. P. RAZELOS and V. PASCHKIS, Blast furnace design—analogue simulation of a blast furnace stove, *Iron Steel Engnr* **43**, 115 (1966).
28. F. W. LARSEN, Rapid calculation of temperature in a regenerative heat exchanger having arbitrary initial solid and entering fluid temperatures. *Int. J. Heat Mass Transfer* **10**, 149 (1967).
29. J. CRANK and P. NICHOLSON, A practical method for numerical evaluation of partial differential equations of the heat conduction type, *Proc. Camb. Phil. Soc. Math. Phys. Sci.* **43**, 50 (1947).
30. I. B. PARKER and J. CRANK, Persistant discretization errors in partial differential equation of parabolic type. *Comput. J.* **7**, 163 (1964).
31. E. L. ALBASINY, On the numerical solution of a cylindrical heat conduction problem, *Q. Jl. Mech. Appl. Math.* **13**, 374 (1960).
32. P. KEAST and A. R. MITCHELL, On the instability of the Crank–Nicholson formula under derivative boundary conditions, *Comput. J.* **9**, 110 (1966).
33. O. A. SAUNDERS and H. J. FORD, Heat transfer in the flow of gas through a bed of solid particles, *J. Iron Steel Inst.* **141**, 291 (1940).
34. Z. F. CHUKANOV and E. A. SHAPATINA, Dynamics of the process of low temperature carbonisation of solid fuel, *Izv. Akad. Nauk. S.S.R. Ord. Tekh Nauk* **7**, 746 (1945).
35. H. HAUSEN, *Warmeübertragüng im Gegenstrom, Gleichstrom, und Kreuztrom.* Springer-Verlag, Berlin (1950).
36. P. J. HEGGS and D. HANDLEY, Momentum and heat transfer mechanisms in regular shaped packings. *Trans. Instn Chem. Engrs*, **46**, T251 (1968).
37. F. A. CRESWICK, A digital computer solution of the equations for transient heating of a porous solid including effects of longitudinal conduction, *Ind. Math.* **8**, 61 (1957).
38. W. TIPLER, A simple theory of the heat regenerator, *Proc. 7th Int. Congr. Appl. Mech.* Section III, p. 196, London (1948).
39. J. W. HLINKA and H. G. LANDAU, Steady State temperature distribution in a counterflow heat exchanger including longitudinal conduction in the wall. *A.S.M.E. Paper* No. 60-WA 0 236 (1960).
40. P. RAZELOS and A. LAZARIDIS, A lumped heat transfer coefficient for periodically heated hollow cylinders, *Int. J. Heat Mass Transfer* **10**, 1373 (1967).
41. G. D. SMITH, *The Numerical Solution of Partial Differential Equations.* Oxford University Press, London (1965).

APPENDIX 1

Components of equations, $\bar{A}\bar{x}(n+1) = \bar{B}(n)$ which represent the set of simultaneous algebraic equations for the intra-particle conduction case at each length step.

$$\bar{A} = \begin{bmatrix} 2+\Delta y & -\Delta y & & & \\ -Mu & 1+M(1+u) & -M & & \\ & -Mv_{k-1} & 1+M & -Mw_{k-1} & \\ & & \ddots & \ddots & \ddots \\ & & & -3M & 1+3M \end{bmatrix}$$

$$\bar{x}(n+1) = \begin{bmatrix} F_g[n+1,i] \\ F[n+1,i,k] \\ F[n+1,i,k-1] \\ F[n+1,i,k-2] \\ \vdots \\ F[n+1,i,0] \end{bmatrix}$$

$$\bar{B}(n)\begin{bmatrix} (2-a)F_g[n+1,i-1]+aF_s[n+1,i-1] \\ MuF_g[n,i]+(1-M+Mu)F[n,i,k]+MF[n,i,k-1] \\ Mv_{k-1}F[n,i,k]+(1-M)F[n,i,k-1]+Mw_{k-1}[n,i,k-2] \\ \vdots \\ 3MF[n,i,1]+(1-3M)F[n,i,0] \end{bmatrix}$$

where

$$u = \Delta s(1+1/k)K_r,$$

$$M = K_r\Delta z/3\Delta s^2$$

$$v_k = (1+1/k)/2,$$

and

$$w_k = (1-1/k)/2.$$

APPENDIX 2

Components of the simultaneous algebraic equations, $\bar{C}\bar{x}(n+1) = \bar{D}(n)$, which represent the longitudinal conduction case with adiabatic boundaries at each time step.

$$\bar{C} = \begin{bmatrix} 1+X+\frac{1}{2}\Delta z & -X & & & & \\ -g_0 & 1-H+X & -X & & & \\ -g_1 & -h_0+X & 1-H+2X & -X & & \\ -g_2 & -h_1 & -h_0+X & 1-H+2X & -X & \\ \vdots & \vdots & \vdots & \vdots & \vdots & \\ -g_{N-1} & -h_{N-2} & -h_{N-3} & h_{N-4} & \cdots -h_0+X & 1-H+X \end{bmatrix}$$

$$\bar{x}(n+1) = \begin{bmatrix} F_s[n+1,0] \\ F_s[n+1,1] \\ \vdots \\ F_s[n+1,N-1] \\ F_s[n+1,N] \end{bmatrix}$$

$$\bar{D}(n) = \begin{bmatrix} \Delta z+(1+X-\frac{1}{2}b)F_s[n,0]+XF_s[n,1] \\ \frac{1}{2}\Delta z(e+F_g[n,1])+(1-\frac{1}{2}\Delta z-2X)F_s[n,1]+X(F_s[n,2]+F_s[n,0]) \\ \frac{1}{2}\Delta z(e^2+F_g[n,2])+(1-\frac{1}{2}\Delta z-2X)F_s[n,2]+X(F_s[n,3]+F_s[n,1]) \\ \vdots \\ \frac{1}{2}\Delta z(e^N+F_g[n,N])+1-\frac{1}{2}\Delta z-X)F_s[n,N]+XF_s[n,N-1] \end{bmatrix}$$

where

$$e = (2-Y\Delta y)/(2+Y\Delta y),$$
$$f = Y\Delta y/(2+Y\Delta y),$$
$$X = \tfrac{1}{2}K_L\Delta z/Y\Delta y^2,$$
$$g_i = \tfrac{1}{2}\Delta z e^i f,$$
$$h_i = \tfrac{1}{2}\Delta z e^i f(e+1)$$

and

$$H = \tfrac{1}{2}\Delta z(f - 1).$$

For the flux boundaries case, the equations $\bar{C}'\bar{x}'(n+1) = \bar{D}'(n)$ differ only in the first and last rows, so that

$$\bar{C}' = \begin{bmatrix} 1 + X(1 + a/K_f) & -X & & \\ \vdots & \vdots & & \\ -g_{N-1} & -h_{N-2} \ldots -h_0 + X & 1 - H + X(1 - a/K_f) & . \end{bmatrix}$$

Résumé—Les équations mathématiques décrivant le transport de chaleur transitoire entre le fluide s'écoulant à travers un lit fixe et ce lit sont formulés pour les situations où il y a une résistance au transport de chaleur dans la phase solide et une conduction thermique à l'intérieur de la phase solide dans la direction de l'écoulement du fluide.

On présente une analyse numérique pour une solution par calculateur de ces équations et une recherche paramétrique des modèles est employée pour montrer que les valeurs de certains groupes sans dimensions apparaissant à partir de la formulation mathématique peuvent être utilisées pour définir la gamme des conditions sous lesquelles les mécanismes de transport de chaleur alternatif sont importants. Les observations expérimentales des profils de température de sortie en fonction du temps qui suivent un changement par échelon de la température du fluide d'entrée ont été comparées avec les profils prédits théoriquement afin de vérifier la validité des modèles mathématiques. Les valeurs critiques des groupes sans dimensions définissant la gamme limite d'applicabilité des différents modèles sont présentées.

Zusammenfassung—Die mathematischen Beziehungen, welche den instationären Wärmeübergang zwischen dem durch ein Festbett strömenden Medium und dem Packungsmaterial des Festbetts beschreiben, werden angegeben für den Fall (1), dass innerhalb der festen Phase kein Wärmetransport zugelassen wird und für den Fall (2), dass Wärmeleitung in der festen Phase in Strömungsrichtung angenommen wird.

Eine numerische Analyse für die Lösung der Gleichungen auf einer Rechenanlage wird angegeben. Die Untersuchung der einzelnen Parameter der Modelle zeigte, dass die Werte verschiedener dimensionsloser Kenngrössen, die sich aus der mathematischen Formulierung ergeben, dazu verwendet werden können, den Bereich von Bedingungen festzulegen, unter denen die beiden oben angegebenen Arten des Wärneaustausches von Bedeutung sind.

Experimentelle Untersuchungen der Zeit- Temperatur-Durchbruchprofile in Abhängigkeit von einer schrittweisen Änderung der Eintrittstemperatur des Strömungsmediums wurden mit den theoretisch vorausberechneten Profilen verglichen, um die Gültigkeit der mathematischen Modelle nachzuprüfen. Die kritschen Werte der dimensionslosen Kenngrössen, welche die Grenzbereiche der Anwendbarkeit der verschiedenen Modelle festlegen, werden angegeben.

Аннотация—Математические уравнения, описывающие нестационарный перенос тепла жидкостью, протекающей через неподвижный слой насадки, сформулированы для случаев, когда (1) существует сопротивление переносу тепла в пределах твердой фазы и (2) в твердой фазе имеет место теплопроводность в направлении движения жидкости.

Представлен численный анализ для решения этих уравнений на машине, и параметрическое исследование моделей применяется для того, чтобы показать, что значения определенных безразмерных групп, возникающих при математической обработке, могут использоваться для определения диапазона условий, при которых важны другие механизмы переноса тепла. Результаты экспериментальных наблюдений за профилями температуры, как функции времени, после ступенчатого изменения температуры жидкости на входе, сравнивались с теоретическими профилями для проверки справедливости математических моделей. Представлены критические значения безразмерных групп, определяющих диапазон применимости различных моделей.